

Hemodynamic Characterization of Localized Aortic Valve Calcifications

Reza Daryani¹^a, Emre Cenk Ersan²^b and M. Serdar Çelebi²^c

¹*Faculty of Mechanical Engineering, Istanbul Technical University, Istanbul, Turkey*

²*Informatics Institute, Department of Computational Science & Eng., Istanbul Technical University, Istanbul, Turkey*

Keywords: Calcification, Aortic Valve, FSI Simulation, Hemodynamic Characterization, Blood Flow.


Abstract: Different hemodynamic characteristics of the blood flow can be studied by numerical simulations of the blood flow around the heart valves, which are significantly useful in various fields such as recognition and prediction of cardiovascular diseases, valve surgery, replacement, and advanced design of patient-specific prosthetic valves. One of these common valvular diseases is aortic valve stenosis, which mainly occurs due to the decreased orifice area between the valves' leaflets and leads to insufficient blood pumping. In the aortic valve, calcification is the main reason for stenosis in which calcium deposits on the leaflets increase their rigidity and consequently prevent them from fully opening and closing. Severe cases of this disease lead to morbidity and mortality. In this work, different localized calcifications of the aortic valve are studied for several grades of this disease and compared with the healthy case. For this purpose, single-phase FSI simulations of blood flow are performed for various degrees of localized calcification patterns and pertinent hemodynamic parameters are obtained. Critical flow parameters, transvalvular indexes and Wall Shear Stress (WSS) based indexes are discussed in detail.


1 INTRODUCTION


One of the most frequent Valvular Heart Diseases (VHD) among the elderly population is Aortic Stenosis (AS) which accounts for 43% of VHD (Pandya, 2012). According to Nudel (2015), 25% of adults over the age of 65 are affected by this disease. The occurrence of this pathological condition is mainly due to the calcium deposition on the aortic valve leaflets and it is characterized by narrowed orifice area of the leaflets. The initiation phase originates in the form of a nodule which grows over time (Halevi et al., 2016). This stage is associated with endothelial damage of the leaflets as a result of higher flow shear and mechanical stresses (Freeman et al., 2005; Otto, 2008). AS is classified into mild, moderate, and severe levels, which are based on the measured Aortic Valve Area (AVA) using Transthoracic Doppler Echocardiography (TDE) analysis (Kappetein et al., 2013). Severe AS cases are followed by morbidity and mortality complications

and its treatment requires aortic valve replacement (Luraghi et al., 2020; Halevi et al., 2018).

Luraghi et al. (2020) worked on the potential complication associated with calcification patterns in Transcatheter Aortic Valve Replacement (TAVR) utilizing FSI models. Sarbandi et al. (2021) developed 2D and 3D FSI models to investigate the role of the bio-transport process in calcification and thrombosis for aortic valves. Their results revealed that there is a close relationship among wall shear stress, flow vortices, and concentration patterns near and far from the leaflets. However, there is a lack of information about the process of 3D calcification formation, flutter dynamics of leaflets and other pertinent hemodynamic factors. So far, numerous studies regarding FSI modelling of the aortic valve calcification have attempted to incorporate the effect of calcification as an increase in the thickness of the valve with the assumption of uniform distribution or the stiffness of the leaflets (Gilmanov et al., 2019; Oks et al., 2022). Gilmanov et al. (2019) conducted a

^a <https://orcid.org/0000-0002-5504-3070>

^b <https://orcid.org/0000-0003-0761-6193>

^c <https://orcid.org/0000-0003-4566-0216>

patient-specific FSI simulation to study the effect of varying leaflet stiffness in transvalvular hemodynamics.

It is reported that the calcification pattern and its growth over time are not random. In an examination of a group of patients with calcified aortic leaflets, it was found that the spatial distribution of calcium deposits has two identified patterns (Thubrikar et al., 1986). The first one is located along the coaptation line of the leaflets and is named the coaptation pattern. The other one is the radial pattern which is seen along the attachment line of the leaflets. Halevi et al. (2015) implemented a new reconstructing technique of 3D-geometry of calcification initiation and growth which confirms the work of Thubrikar et al. (1986). They found that calcification patterns strongly affect the mechanical flexibility of the leaflets and also their orifice area. Halevi et al. (2016) analyzed the hemodynamic effect of 3D patient-specific calcification patterns of the aortic valve by using Fluid-Structure Interaction (FSI) simulations. Their results revealed that the presence of calcific deposits dramatically influences the flow shear stresses. Although it has paved the way to study the hemodynamic effect of calcification patterns, there is little focus on other hemodynamic parameters, such as wall shear stress-based analysis.

In this study, we developed computational 3D models of the calcified aortic valve using the FSI approach within an Immersed Boundary (IB) framework combined with Finite Element (IBFE) (Griffith and Luo, 2017). Simulations were established based on 3D geometries for different grades of deposition accumulation, which can be classified as Grades 1-6. The results are obtained and analyzed for a single aortic flow condition where aortic pressure fluctuates around 120-80 mmHg for the healthy case. For graded cases, while outflow pressure is identical to the healthy case, inflow pressure increases with the severity of the calcification grade. Quantification of the critical parameters in blood flow is performed by using numerous transvalvular hemodynamic and WSS-based indexes. Additionally, the effect of deposition patterns on the vortical structures of the flow field is investigated. The influence of calcification severity on aortic valves is studied by using transvalvular hemodynamic indexes such as energy loss, aortic jet velocity, kinetic energy and the average magnitude of the velocity. To the authors' best knowledge, this is the first attempt to discuss the comprehensive hemodynamic characterization of localized aortic valve calcification using a range of calcification grades.

2 MATERIAL AND METHODS

The mathematical model of our hemodynamic FSI coupling algorithm will be discussed first, then model geometry and further details in the numerical scheme and boundary conditions will be presented.

2.1 Mathematical Modeling

The FSI approach we used is based on the IBFE formulation proposed by Griffith and Luo (2017). Deformation, elasticity and stresses of the immersed structure are described by a Lagrangian form, while the Eulerian form is used to describe the incompressible Navier-Stokes equations. Let $\Omega \in \mathbb{R}^3$ and $\mathbf{x} = (x, y, z) \in \Omega$ denote the physical domain for the coupled fluid-structure system and the corresponding Cartesian coordinates, respectively. Let $U \in \mathbb{R}^3$ denote the initial coordinate system for the structure, represented by the curvilinear Lagrangian coordinates $(q, r, s) \in U$. At time t , $\chi(\mathbf{X}, t)$ describes the position of the material point \mathbf{X} ; then, the structure and the fluid occupy the regions $\chi(U, t) = \Omega_s$ and $\Omega_f(t) = \Omega \setminus \Omega_s$ at time t , respectively.

The equations of motion for the coupled fluid-structure system in IB form are:

$$\rho \left(\frac{\partial \mathbf{u}}{\partial t}(\mathbf{x}, t) + \mathbf{u}(\mathbf{x}, t) \cdot \nabla \mathbf{u}(\mathbf{x}, t) \right) = -\nabla p(\mathbf{x}, t) + \mu \nabla^2 \mathbf{u}(\mathbf{x}, t) + \mathbf{f}(\mathbf{x}, t) \quad (1)$$

$$\nabla \cdot \mathbf{u}(\mathbf{x}, t) = 0 \quad (2)$$

$$\mathbf{f}(\mathbf{x}, t) = \int_U \mathbf{F}(\mathbf{X}, t) \delta(\mathbf{x} - \chi(\mathbf{X}, t)) d\mathbf{X} \quad (3)$$

$$\frac{\partial \chi}{\partial t}(\mathbf{X}, t) = \mathbf{u}(\chi(\mathbf{X}, t), t) = \int_{\Omega} \mathbf{u}(\mathbf{x}, t) \delta(\mathbf{x} - \chi(\mathbf{X}, t)) d\mathbf{x} \quad (4)$$

Eqs. 1 and 2 are the incompressible momentum and continuity equations, where ρ and μ are the density and the dynamic viscosity, $\mathbf{u}(\mathbf{x}, t)$ and $p(\mathbf{x}, t)$ are the Eulerian velocity and pressure fields, and $\mathbf{f}(\mathbf{x}, t)$ is a body force term representing the Eulerian elastic force density which is applied to the fluid by the structure. Eqs. 3 and 4 describe the interaction between the Lagrangian and Eulerian domains by integral transformation with a Dirac delta function $\delta(\mathbf{x}) = \delta(x)\delta(y)\delta(z)$ in three dimensions. Eq. 3 defines the conversion of Eulerian elastic force

density $f(\mathbf{x}, t)$ into the Lagrangian elastic force density $\mathbf{F}(\mathbf{X}, t)$, while Eq. 4 specifies the no-slip condition of the viscous fluid on the fluid-structure interface.

2.2 Model Geometry

The geometry of the healthy aortic valve is illustrated in Figure 1. The primary CAD model is obtained from work of Wang (2015) and the ascending aorta section is added as a straight tube for the sake of simplicity. The housing height in Figure 1 is 0.116 m with an inlet diameter of 0.025 m and a wall thickness of 0.001 m. The height of the aortic valve is 0.015 m and its uniform thickness is 0.0005 m.

As stated in the work of Thubrikar et al. (1986), the locations of deposits are not random and they gradually develop along the coaptation line or near to the aortic root. Based on the work of Bahler et al. (1999), the severity of the calcification can be classified into several grades, which are described as:

- Grade 1 represents no calcification,
- Grade 2 represents the localized area of increased reflectivity but no areas of dense calcification,
- Grade 3 represents markedly increased reflectivity (calcification) in one leaflet but equal to or less than Grade 2 changes in other leaflets,
- Grade 4 represents markedly increased reflectivity in two leaflets but equal to or less than Grade 2 changes in the third leaflet,
- Grade 5 represents moderately increased reflectivity in all leaflets,
- Grade 6 represents severely increased reflectivity in all leaflets.

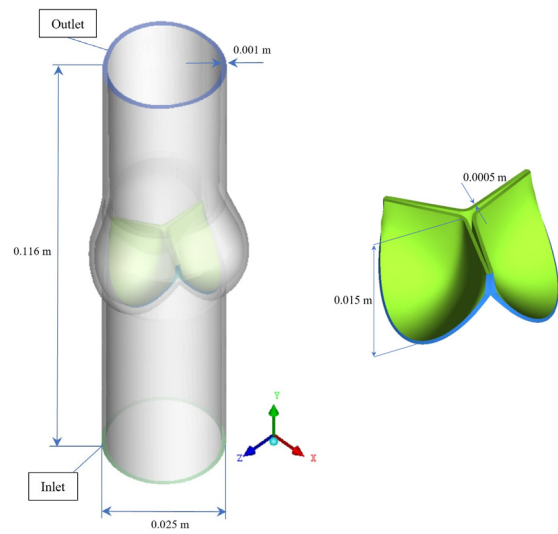


Figure 1: Reference geometry of the aortic valve for all calcification models.

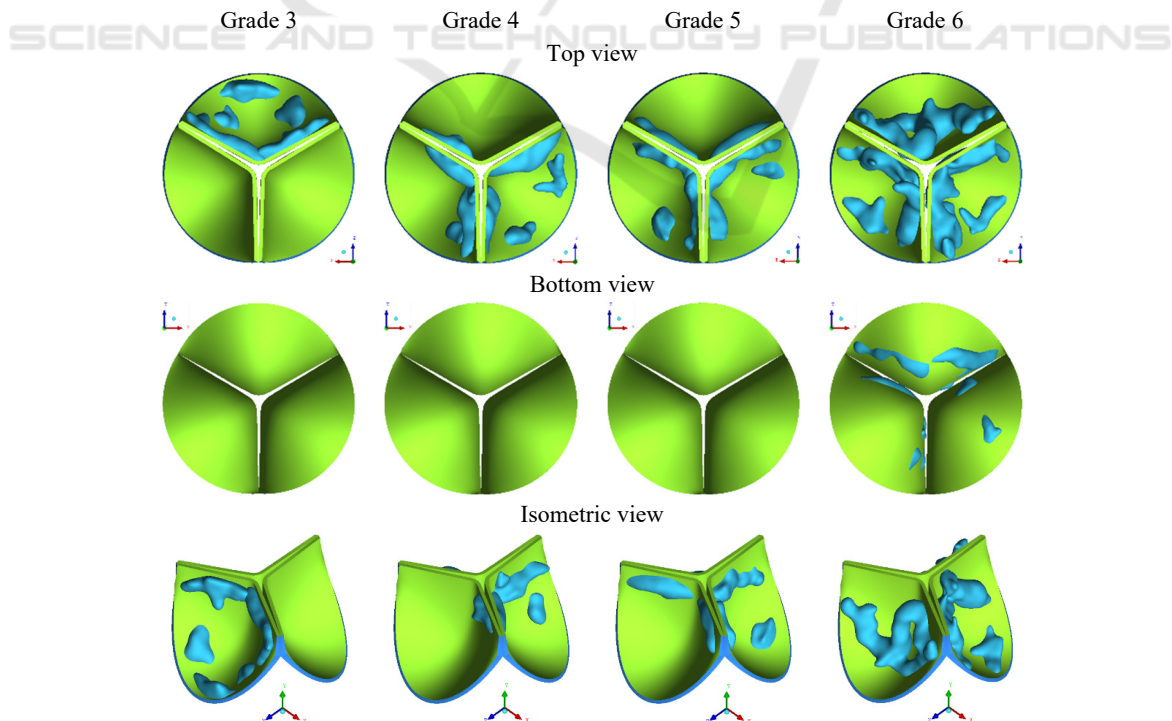


Figure 2: Geometries of the calcification grades merged with the reference aortic valve geometry.

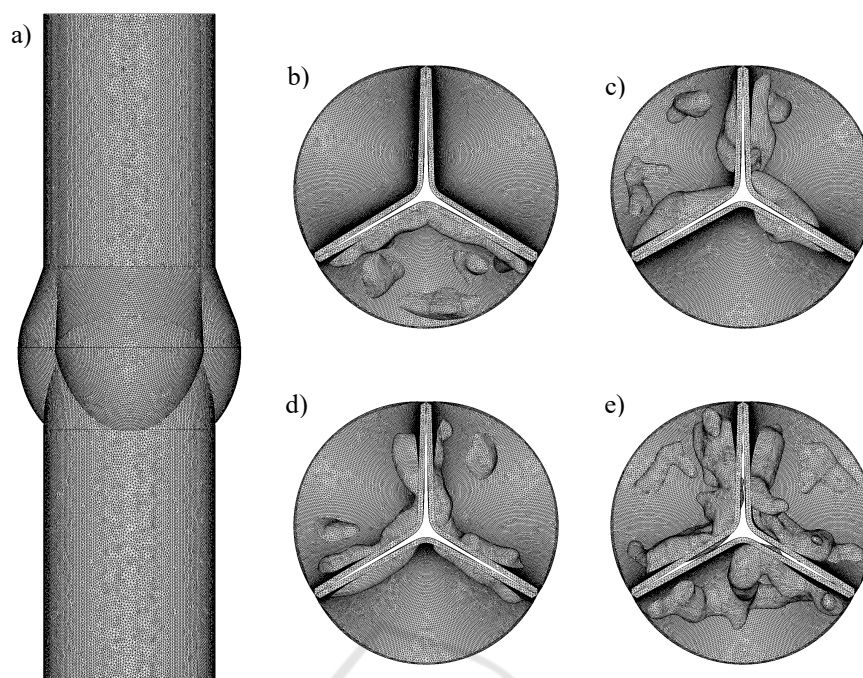


Figure 3: Illustration of the unstructured mesh of a) housing, b-e) each valve of Grades 3-6, respectively.

Due to the lower impact of Grade 2 calcification, we ignored this grade in our simulations and the geometries were created for Grades 3-6. Calcification geometries are adopted from the 3D geometries in the work of Lavon et al. (2019) and they were merged with our reference geometry of the aortic valve model. Model geometries are generated based on the patterns using medical classifications presented in the work of Bahler et al. (1999) for several grades, which are illustrated in Figure 2. It should be noted that the geometry of Grade 6 is the only case where the calcific deposition is visible from the bottom view (see in Grade 6 in Fig. 2).

2.3 Numerical Schemes and Boundary Conditions

The fluid mesh treatment of our IB method uses a staggered, block-structured fixed Cartesian grid to discretize the Eulerian variables, velocity, pressure and force density (Griffith, 2017). The divergence, gradient, and Laplace operators are approximated using standard second-order accurate finite difference methods (Griffith, 2009). A version of the piecewise parabolic method (PPM) is used to discretize the convective term in momentum equation (Colella et al., 2017). The Lagrangian variables associated with the immersed structure are discretized using an unstructured finite element mesh.

2.3.1 Structure Mesh

Figure 3a represents the reference housing and in Figures 3b-e, the structure meshes of each grade are illustrated. For whole structure mesh, unstructured first-order tetrahedral elements are used. The total number of structure mesh elements are 1.89, 1.88, 1.93 and 2.12 million for Grades 3-6, respectively. For healthy case, the number of mesh elements is 1.86 million.

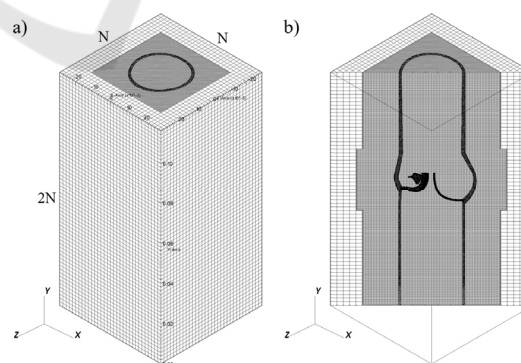


Figure 4: Computational mesh for the calcified aortic valve model, a) Isometric view, b) Cross-diagonal section view.

2.3.2 Fluid Mesh

The fluid domain is considered as a Cartesian box and discretized by $N \times 2N \times N$ mesh elements in x , y , and z directions, respectively. A static mesh refinement level with a refinement ratio of 2 is used near the immersed interface, as shown in Figure 4. In the simulations, N is taken as 64, which leads to a total fluid mesh of about 2.15 million mesh elements with the dimensions of $0.058 \text{ m} \times 0.116 \text{ m} \times 0.058 \text{ m}$.

2.3.3 Constraints and Boundary Conditions

The housing structure is anchored to the top and bottom surfaces of the physical domain. This is done by assigning integer numbers to each surface in ICEM CFD® software during the meshing process, then imposing zero displacement constraints on the top and bottom surfaces of Figure 4. Wall boundary conditions are applied on the bottom and top boundaries. For the side boundaries of the physical domain, zero tangential velocity and zero normal velocity gradient conditions are employed. In Figure 5, the velocity profile is used as the inflow and the pressure profile is implemented as the outflow boundary condition on the circular domains located at the bottom and top walls of the computational box, respectively.

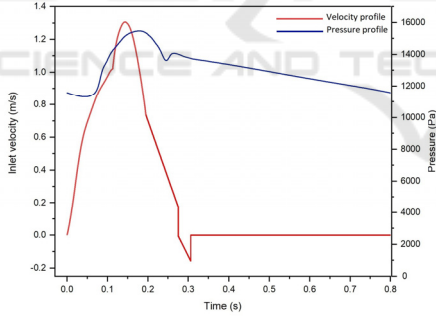


Figure 5: The inflow and outflow boundary conditions for the calcified aortic valve model, a) Inlet velocity profile (Spühler et al., 2018), b) Outlet pressure profile (Rubenstein et al., 2015).

2.3.4 Numerical Implementation

An explicit version of Crank Nicolson–Adams Bashforth scheme is employed for time stepping with a step size of $\Delta t = 1.0 \times 10^{-5} \text{ s}$. Blood is modeled as a single-phase Newtonian fluid with a dynamic viscosity and density of $0.0035 \text{ Pa}\cdot\text{s}$ and 1056 kg/m^3 , respectively. The flow is transient and the simulations are performed initially for one cardiac cycle (0.8 s).

We used the open source IBAMR software framework (<https://ibamr.github.io/>) for our models. Simulations run on The National Center of High-Performance Computing of Turkey (UHcM). We used InfiniBand®-based (FDR, 56 Gbps) computing cluster with two compute nodes, each consisting of an Intel® 2.4 GHz Xeon® E5-2680 v4 processor with 28 cores and 128 GB of memory. We observed a parallel speedup factor of nearly 1.5 by doubling the number of processors in up to two nodes (56 cores). However, by employing three nodes, the parallel performance reduces due to network communication and high frequency parallel I/O. So we decided to employ two compute nodes due to the performance/cost ratio. Each simulation took approximately 200 hours of wall clock time. The typical total CPU hours for each simulation was around 11500.

2.3.5 Material Model

As the material model of the aortic valve, a Neo-Hookean hyper-elastic model is used and its strain energy distribution function is given as

$$\mathbf{W} = \frac{\mu}{2}(I_1 - 3) - \mu \ln(\det(F)) + \frac{\lambda}{2}(\ln(\det(F)))^2 \quad (5)$$

where λ , μ are the Lamé constants of linear elasticity and F is the deformation gradient. In our model, the aortic valve and the housing are considered to be incompressible ($\det(F) = 1$).

1st Piola–Kirchhoff stress tensor can be written as

$$\mathbb{P} = \mu F + [\lambda \ln(\det(F)) - \mu] F^{-T} \quad (6)$$

The housing is modeled as a semi-rigid tube. Calcified deposits are modeled as a linear elastic material with Young's modulus of 2 MPa and Poisson's ratio of 0.45. 1st Piola–Kirchhoff stress tensor for a linear elastic model is

$$\mathbb{P} = \mu(F + F^{-T} - 2I) + \lambda \text{tr}(F - I)I \quad (7)$$

The list of material parameters is given in Table 1.

Table 1: Material properties for the calcified aortic valve models.

Part	Material model	Parameters
Aortic valve	Neo-Hookean	$\mu = 140 \text{ kPa}$ $\lambda = 17 \text{ MPa}$
Calcifications	Linear elastic	$E = 2 \text{ MPa}$ $\nu = 0.45$

3 NUMERICAL RESULTS AND HEMODYNAMIC CHARACTERIZATION OF CALCIFIED AORTIC VALVE

The calcification of leaflets can result in their deterioration and remodeling, which in turn leads to a shorter life span of the Bioprosthetic Heart Valve (BHV) and, in general, reduces the functionality of a valve. Subsequent changes in transverse pressure gradients and shear forces may lead to further complications, which make localized calcifications necessary to be investigated. Thus, hemodynamic alteration in the aortic valve region due to calcification plays a key role in problems associated with VHD. In the following sections, the flow patterns for various calcification grades and underlying hemodynamic parameters divided into Transvalvular hemodynamic and Wall Shear Stress (WSS) based indexes will be discussed.

3.1 Analysis of Flow Pattern

For a better understanding of the calcification effects on valve leaflets, at first, velocity vectors of flow around healthy aortic valve will be compared with the calcified cases shown in Figure 6. Initially, the leaflets remain closed until the pressures are equalized on the ventricular and aortic sides. When the pressure increases on the ventricular side, the valve starts to open around $t = 0.02$ s. The valve opens in a form with a fully circular orifice area before the velocity reaches its peak at the systole phase. The blood moves through the valve into the ascending aorta without any significant flow deformation until this time instant. After the peak systole, when the jet velocity decreases, several vortices are generated due to the flow separation from leaflet tips. When the jet velocity approaches zero during the late systole, the leaflet closure occurs due to the backflow into the Valsalva sinus region filling the valve packets as a result of the hemostatic effect. Arantius nodules and coaptation lines are observed to be well aligned spatially and temporally. As expected, no flow is observed behind the leaflets during the opening phase. However, vortical flow patterns can be seen within the packets when the valve closes. In the final figure at $t = 0.30$ s, some regurgitation is observed in the middle area close to the Arantius nodules of all three leaflets.

As stated in Section 2.2 before, Grade 3 represents the case that only one leaflet is involved with calcification. Due to relatively increased valve

stiffness as a result of calcification, leaflets undergo a sudden opening with a delay. However, in healthy case valves open earlier and the slope of the velocity increment is smoother. Therefore, at the beginning of the systole blood velocity is higher in healthy case. Blood flow passes the valve orifice in a spatially asymmetric manner due to unstable displacement of one leaflet. This asymmetry shifts the flow towards the ascending aorta wall and diverges from symmetric flow which the healthy case has. As a result of this deflection, flow circulates toward the calcified leaflet which can be seen in the plots of $t = 0.15, 0.185$ s. This flow circulation contributes to an earlier closure of the calcified leaflet that is shown in plots of $t = 0.27, 0.30$ s. In the healthy aortic valve, the jet flow passing the orifice retains its uniform shape; however, the constrained leaflet disturbs the flow and thus the jet flow becomes chaotic. While healthy aortic valve closes by the end of $t = 0.30$ s, Grade 3 calcified valve closes with a slight delay.

In Grade 4 calcified aortic valve, two leaflets have notable calcium deposits on their upper surface facing to ascending aorta. More intense calcification leads to more valve resistance which results in a lower orifice area and increased jet velocity. Furthermore, the jet becomes narrower and centric whereas it is more uniformly distributed for the healthy case. In contrast to Grade 3, in the Grade 4, the flow is more centric in the systole phase, but due to the earlier closure of the strongly calcified two leaflets, the flow deviates. This shifts the blood flow toward the third leaflet which can be observed in figures of $t = 0.27, 0.35$ s. This flow deviation creates a strong vortex in the ascending aorta region, and this leads to a higher energy dissipation.

By comparing the results of the velocity vectors for the blood flow of Grade 5 with previous cases, it is seen that increasing calcification severity leads to a stronger jet flow and unstable closure of leaflets. Also, due to the reduced orifice area, the jet flow width becomes smaller. In Grade 5 case, deposit distribution is almost symmetric and we observe an almost symmetric blood flow comparing to Grade 4. The leaflet with no deposit, takes a concave form in early systole phase and during the valve closure in the late systole phase, it deviates the flow toward the ascending aorta wall. The resulting collision creates vortices in the ascending aorta after valve closure. Grade 6 calcification case is the most severe one and as expected the strongest jet flow is observed. In comparison with the Grade 3 case, there is an increase of about 25% in the jet velocity magnitude. The length and duration of the aortic jet are measured maximum due to the smallest Geometric Orifice Area

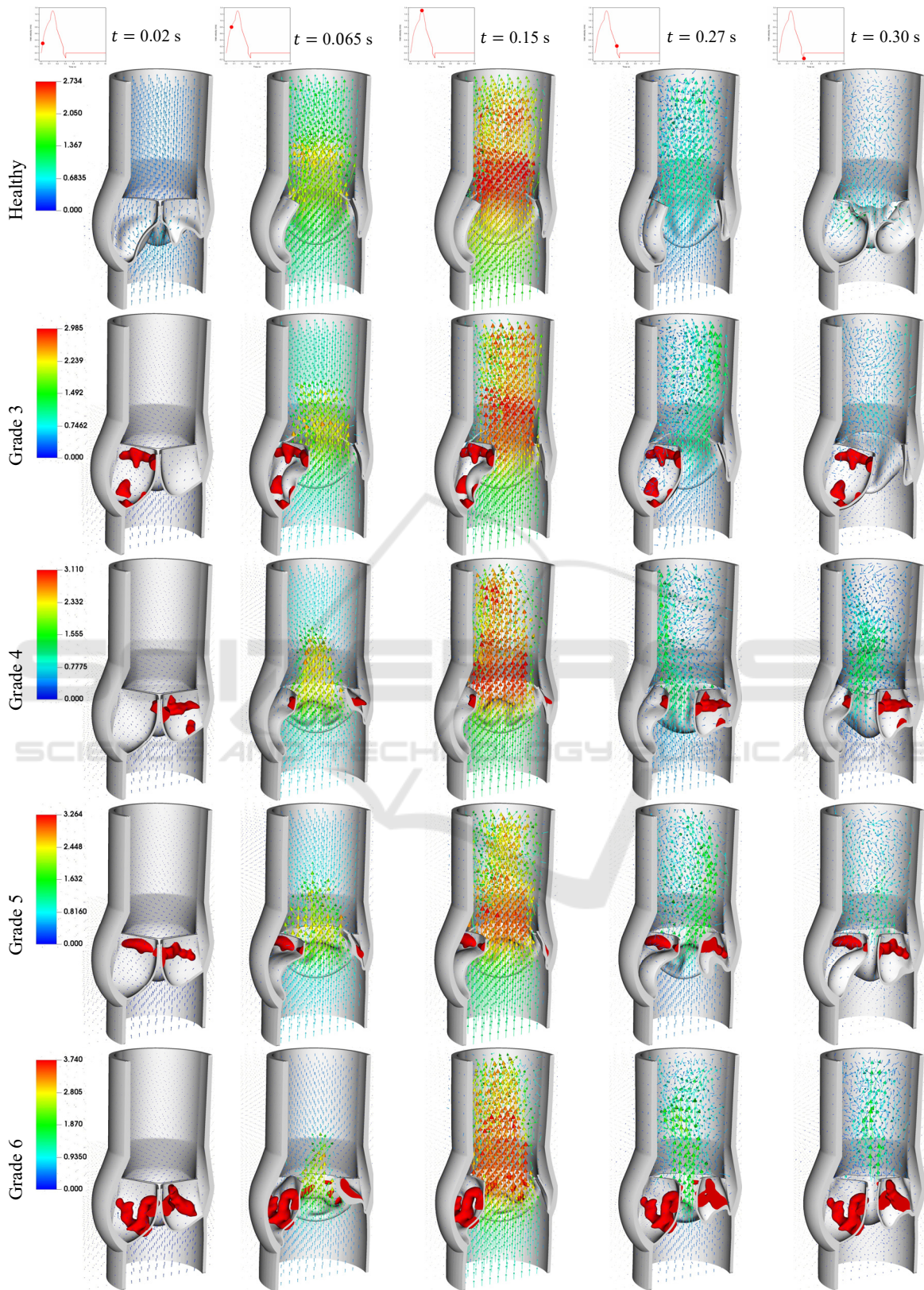


Figure 6: Illustration of flow vectors [m/s] at different times over a cardiac cycle for various calcification cases.

(GOA) where jet width is minimum. The relatively symmetric distribution of the deposits on all three leaflets, their opening and closure is almost symmetrical. However, the latest valve opening is observed with the smallest GOA generating the strongest vortex structures. Because of the narrower jet flow, the strongest backflow circulations toward the leaflets are observed in the ascending aorta.

3.2 Transvalvular Hemodynamic Index Analysis

Disturbed hemodynamics of unsteady aortic flow in the presence of localized calcifications can be characterized by some hemodynamic parameters that are utilized in the early detection of valvular heart diseases. Calcification affects the aortic valve kinematics and reduces its functionality by decreasing the amount of blood passed through the leaflets.

Variation of the GOA in healthy and calcified aortic valves for a time range of half a cardiac cycle is given in Figure 7. Based on the published clinical data by Thubrikar (1990), the Aortic Valve Area of a healthy aortic valve is within the range of $3.9 \pm 1.2 \text{ cm}^2$ and our results for the healthy case agree and align with this range.

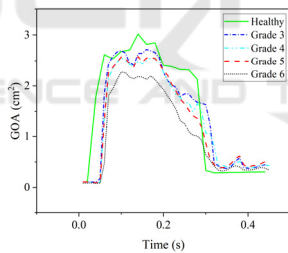


Figure 7: Geometric orifice area (GOA) variation for the healthy and calcified aortic valve in a half-cardiac cycle.

It can be observed that calcification greatly affects leaflet openings and the resulting orifice area reduction is remarkable. Results show that, with the increased calcification, openings of the valve leaflets are delayed. In the healthy aortic valve, leaflets opening occurs around 0.02 s; however, for the diseased cases opening time is about 0.05 s. The main reason for this is the increased resistance of calcified leaflets. In the healthy aortic valve case, the GOA profile follows the trend of the inlet profile where the orifice area increases until the peak systole and decreases until valve closure. In contrast, the trend of the calcified cases is completely different and there is a sudden reduction at nearly 0.13 s. Additionally, by comparing the GOA curves of the calcified cases, it

can be observed that by increasing the calcification intensity, leaflets closure occurs more gradually. Similar to the delay in the opening phase, the delay in the closure of the leaflets is observable for the calcified cases. Furthermore, in these cases, there are increments in the GOA after the valve closure referring to a severe delay in the closing of coaptation lines. In this situation, severe regurgitation occurs due to the closing delay of the valve leaflets, resulting in insufficient blood flow to the ascending aorta. In the diseased cases, the increased stiffness of the leaflets leads to increasing ventricle pressure resulting in small inflation at the bottom section of the model wall. As stated, by looking at the GOA curves of the calcified cases, there is an increment after about 0.36 s. One of the reasons for this bump might be the depletion of the stored fluid volume in the inflated section of the model wall even after the early diastole.

Another transvalvular hemodynamic parameter is the maximum velocity, V_{max} , of the jet passing through the aortic orifice area. By using this parameter, pressure drop across the valve can be calculated using the simplified Bernoulli equation. In Figure 8, the maximum velocity of flow passing through the orifice area for healthy and calcified cases is given. Results show that increasing the calcification severity directly raises the jet velocities due to the decreased orifice area to maintain the flow rate.

One important observation is the early drop of jet velocity near $t = 0.2 \text{ s}$ at Grade 4 where two leaflets are constrained by deposit and the third one is free to move. This result reveals that calcification severity is not the only reason for the velocity increment and divergence but also pattern asymmetry plays an important role.

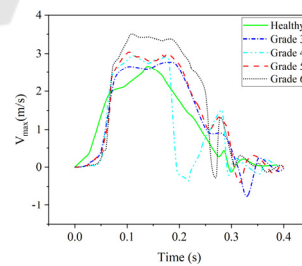


Figure 8: The variation of the maximum jet velocity V_{max} for healthy and calcified valves in a half cardiac cycle.

The third transvalvular hemodynamic parameter is the rate of energy dissipation. This parameter determines the instantaneous power loss of blood flow. It is measured in Watts and can be calculated by $E_{diss} \dot{(t)} = \frac{dE_{diss}}{dt(t)} = \int \Phi dV$. In this equation, $\Phi =$

$\tau \otimes \nabla v$ represents a dissipation function where τ is the viscous shear stress tensor, and $E_{diss}(t)$ is the power loss in the Valsalva sinus region and the following ascending aorta. This parameter explains the shear-related energy dissipation due to the viscous blood flow and the presence of aortic stenosis. The variation of this parameter over a half-cardiac cycle is presented in Figure 9.

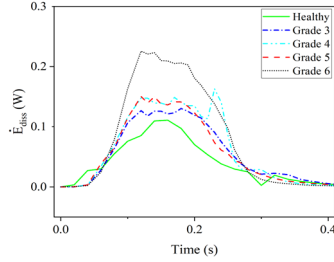


Figure 9: The variation of rate of energy loss for healthy and calcified valve models in a half cardiac cycle.

These results prove that the increasing severity of the stenosis as a result of aortic valve calcification leads to a higher energy dissipation of the blood flow. The value of energy dissipation for the healthy case, in general, is minimum among all cases due to the least resistance to blood flow. For Grade 3 at peak systole, an increase of 10% in energy dissipation is seen in comparison with the healthy case. For Grades 4 and 5 the results are close to each other which implies that the rate of energy loss for higher calcification on two leaflets is similar to the rate of moderate calcification on the three leaflets. The sudden increase in the late systole for Grade 4 might be due to the higher flutter of the leaflets during their closure phase and consequently the creation of the strong vortices that lead to a higher energy dissipation. The highest energy dissipation belongs to the Grade 6 case which is the severe stenosis disease and energy dissipation is doubled in comparison with the healthy aortic valve.

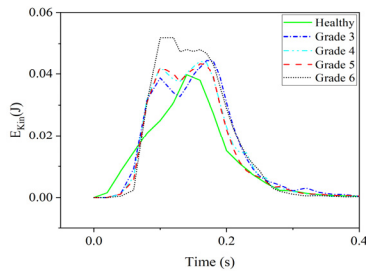


Figure 10: The variation of the kinetic energy (E_{kin}) of the blood flow in a half cardiac cycle for a healthy and calcified aortic valve.

The kinetic energy of the blood flow is the other important hemodynamic parameter and can be determined by $E_{kin}(t) = \frac{1}{2} \rho_f \int_V v^2 dV$ which is directly integrated over the aorta's volume. E_{kin} describes the mechanical energy of the blood flow, which is exchanged with pressure and the viscous dissipation terms. In Figure 10, this parameter is illustrated for healthy and calcified cases. Similar to the previous hemodynamic parameters, increasing the severity of the calcification tends to increase the amount of kinetic energy which leads to an increased energy dissipation and decreased pressure drop.

The last transvalvular hemodynamic index is the average magnitude of the vorticity which is measured in the volume of aorta. The magnitude of vorticity can be quantified using $\Omega_a(t) = \left(\frac{1}{V}\right) \int_V |\Omega| dV$, where $|\Omega| = \sqrt{w_x^2 + w_y^2 + w_z^2}$, $\Omega = (\nabla \times v)$. Figure 11 shows that the vorticity structure of the blood flow is amplified by increasing the severity of the calcification. Similar to the other parameters Grade 6 has the highest values except opening and closing phases of the valve leaflets. In other words, high amount of calcification results in the generation of the strong vortices which leads to a larger energy dissipation rate at time interval $t = 0.05 - 0.30$ s. In comparison with healthy case in which the vorticity magnitude increases until peak systole and decreases after it, the value of this parameter changes within a narrow range after valve opening until the beginning of late systole phase at about $t = 0.30$ s. One main reason for this is that the valve leaflets start to flutter at this time range and generate strong vortices at their tip region.

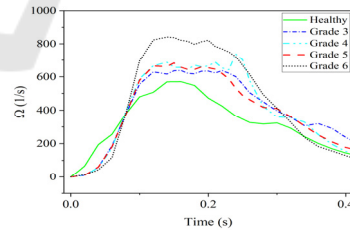


Figure 11: History of vorticity (Ω_a) calculated for healthy and different calcified valves over a half cardiac cycle.

3.3 WSS Based Hemodynamic Index Analysis

In general, hemodynamic parameters and/or indexes can be used for quantifying some cardiovascular diseases. An important group of these parameters can be classified as the Wall Shear Stress (WSS) based hemodynamic indexes. The viscous stresses exerted on the wall surface by the fluid is explained by WSS,

$|\text{WSS}| = n_i \cdot \tau_{ij}$ where n_i is surface normal vector and τ_{ij} is viscous stress tensor. In this work, we will be discussing the results of Time Averaged Wall Shear Stress (TAWSS), Oscillatory Shear Index (OSI), Relative Residence Time (RRT), and Transverse Wall Shear Stress (transWSS) indexes for different cases of the healthy and calcified aortic valves.

Comparing the results of healthy and calcified aortic valve cases in Figure 12, it is observed that the growth of the calcification deposits increases the value of TAWSS both at the edges of the leaflets and the radial region. Furthermore, the intensity of the calcification also leads to an increase in TAWSS. By investigation of the results in Grade 3, it can be observed that TAWSS reaches to higher values at the tip of the non-calcified leaflets. This is caused by the shear loads as a result of the extra transverse pressure gradient fluctuations and by the fluttering movement as a result of the limited opening of the calcified leaflets. In other grade cases, TAWSS values are slightly increased with the larger volume of deposits and spatially span more area. One of the reasons for this is that the shear stress rises at the tips of the leaflets as a result of the higher jet velocity and sharper pressure fluctuations which occur due to the narrowing of the orifice area.

OSI index has a scalar ranging between 0 and 0.5, and it is used to determine whether a flow is laminar (unidirectional) or oscillating (turbulent). The critical point to know is that it does not give any information about the actual magnitude of the oscillation. Figure 12 shows that there is a significant WSS oscillation on the surfaces of the valve leaflets. Additionally, relatively lower OSI values can be observed on surfaces with large calcification deposits. On the other hand, OSI values are relatively lower in the root regions of healthy case.

Relative RRT represents the relative duration that blood resides close to a wall in one cardiac cycle. Comparing the RRT results, it is seen that maximum values appear at the roots of the leaflets and minimum values are at the edges of the leaflets due to the short residence time of blood in this region. Additionally, increasing the calcification level leads to an increase in the RRT values and the maximum values are observed in the Grade 6 case. For each case, RRT values appear to be particularly higher in the root regions of the calcified leaflets. This means that the blood stays for a relatively long time behind the calcification deposits.

The final WSS based hemodynamic index studied is the transWSS, which is defined as the average of WSS components perpendicular to the temporal mean WSS vector over a cardiac cycle. By observing the top views given in the last column of Figure 12, the

presence of calcification slightly increases the transWSS values. For example, in Grade 3, transWSS values on calcified leaflets are slightly higher compared to the healthy leaflets. As it is known, transWSS basically looks at the variation of stresses in lateral directions perpendicular to the main flow direction. Therefore, increase in transWSS occurs due to the greater lateral load components as a result of temporally and spatially unstable fluctuations in cases with increasing generally asymmetric patterned calcifications.

4 DISCUSSION

In this study, we developed an FSI model for the aortic valve and investigated the effect of several grades of localized calcifications. For the first time in the literature, a comprehensive hemodynamic characterization is conducted for an aortic flow in the presence of medically graded localized calcifications. We conducted three stage analysis: analysis of flow pattern, study of transvalvular hemodynamic indexes and WSS based index analysis.

Our initial results showed that increasing calcification severity leads to a stronger jet flow and unstable closure of leaflets. However, we also observed that asymmetric pattern of the localized calcifications may lead to a spatially and temporally unstable behavior of the valve leaflets even if calcification volume is not larger. Due to the reduced orifice area, the jet flow width becomes smaller and blood flow passes the valve orifice as spatially asymmetric flow due to unstable displacement of leaflets. This asymmetry shifts the flow towards the ascending aorta wall and exposes the wall to a higher wall shear stress for a limited period of time. But this periodical WSS impact may lead to erode of endothelial surface of ascending aorta with time. With the increasing calcification grades opening of the valves are delayed, flow velocities significantly increased due to the limited GOA and severe chaotic flow in ascending aorta are observed at the late systole phase. This flow regime generates a significant back flow and recirculation to a Valsalva sinus and root region of the valve. Another potential effect of this flow is the redirection of the feeding flow at the right and left coroner artery entries. It is clear that there is a need for further analysis of this back flow effect locally on the right and left coroner entry zones whether the rate of blood flow is reduced or not. Another important finding in this study is to observe a higher energy dissipation of blood flow due to the increasing severity of aortic valve calcification.

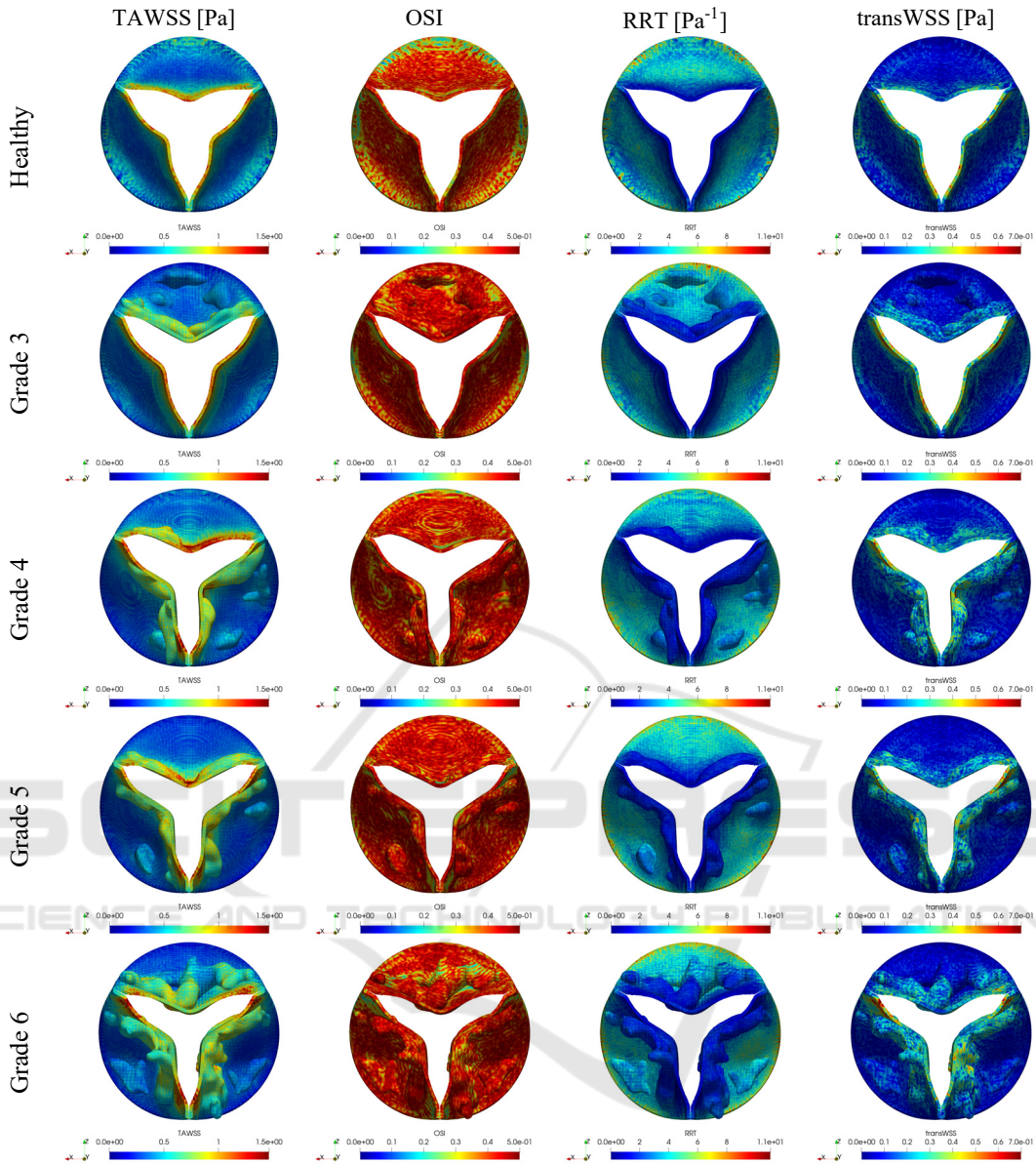


Figure 12: WSS based hemodynamic indexes for healthy and different grade calcification cases.

The variation of the maximum jet velocity V_{max} is also align with the energy dissipation behaviour of blood flow which is exposed to a higher resistance. Similarly, increasing severity of the calcification tends to increase both the amount of kinetic energy and the vorticity structure of the blood flow which lead to an increased energy dissipation and decreased pressure drop. TAWSS and OSI indexes show that growth in localized calcification leads to an increase of these two indexes. WSS values are mostly increased at the edges of the leaflets and flow oscillations occur everywhere in the Valsalva sinus compared to healthy case. Moreover, residence time

of the blood slightly increased at the root region but significantly reduced at the edges of the leaflets. When we combine low TAWSS and transWSS with high RRT, we can conclude that the root region may be a good candidate for further formation of the stasis which is the initial stage of thrombosis according to the low shear stress theory. Similarly, combination of high TAWSS, OSI and transWSS may lead to a thrombosis formation at the edges of the valves based on the high shear stress theory.

For a future work, two and more phase FSI blood flow models are needed to observe RBC and platelet

aggregations around both back region of the aortic valve and edges of the leaflets.

ACKNOWLEDGEMENTS

This work is funded by the Scientific and Technological Research Council of Turkey (TUBITAK) as ARDEB 1001 project under the grand number 120M671. Computing resources used in this work were provided by the National Center for High-Performance Computing of Turkey (UHeM) under grant number 5010662021.

REFERENCES

- Bahler, R. C., Desser, D. R., Finkelhor, R. S., Brener, S. J., & Youssefi, M. (1999). Factors leading to progression of valvular aortic stenosis. *The American journal of cardiology*, 84(9), 1044-1048.
- Colella, P., & Woodward, P. R. (1984). The piecewise parabolic method (PPM) for gas-dynamical simulations. *Journal of computational physics*, 54(1), 174-201.
- Freeman, R. V., & Otto, C. M. (2005). Spectrum of calcific aortic valve disease: pathogenesis, disease progression, and treatment strategies. *Circulation*, 111(24), 3316-3326.
- Gilmanov, A., Barker, A., Stolarski, H., & Sotiropoulos, F. (2019). Image-guided fluid-structure interaction simulation of transvalvular hemodynamics: Quantifying the effects of varying aortic valve leaflet thickness. *Fluids*, 4(3), 119.
- Griffith, B. E. (2009). An accurate and efficient method for the incompressible Navier–Stokes equations using the projection method as a preconditioner. *Journal of Computational Physics*, 228(20), 7565-7595.
- Griffith, B. E., & Luo, X. (2017). Hybrid finite difference/finite element immersed boundary method. *International journal for numerical methods in biomedical engineering*, 33(12), e2888.
- Halevi, R., Hamdan, A., Marom, G., Mega, M., Raanani, E., & Haj-Ali, R. (2015). Progressive aortic valve calcification: three-dimensional visualization and biomechanical analysis. *Journal of biomechanics*, 48(3), 489-497.
- Halevi, R., Hamdan, A., Marom, G., Lavon, K., Ben-Zekry, S., Raanani, E., ... & Haj-Ali, R. (2016). Fluid–structure interaction modeling of calcific aortic valve disease using patient-specific three-dimensional calcification scans. *Medical & biological engineering & computing*, 54, 1683-1694.
- Halevi, R., Hamdan, A., Marom, G., Lavon, K., Ben-Zekry, S., Raanani, E., & Haj-Ali, R. (2018). A new growth model for aortic valve calcification. *Journal of Biomechanical Engineering*, 140(10), 101008.
- IBAMR. Immersed Boundary Method Adaptive Mesh Refinement Software Infrastructure. Available at: <https://ibamr.github.io/>. Accessed 10 January 2021.
- Kappetein, A. P., Head, S. J., Généreux, P., Piazza, N., Van Mieghem, N. M., Blackstone, E. H., ... & Leon, M. B. (2013). Updated standardized endpoint definitions for transcatheter aortic valve implantation: the Valve Academic Research Consortium-2 consensus document. *The Journal of thoracic and cardiovascular surgery*, 145(1), 6-23.
- Lavon, K., Marom, G., Bianchi, M., Halevi, R., Hamdan, A., Morany, A., ... & Haj-Ali, R. (2019). Biomechanical modeling of transcatheter aortic valve replacement in a stenotic bicuspid aortic valve: deployments and paravalvular leakage. *Medical & biological engineering & computing*, 57, 2129-2143.
- Luraghi, G., Matas, J. F. R., Beretta, M., Chiozzi, N., Iannetti, L., & Migliavacca, F. (2020). The impact of calcification patterns in transcatheter aortic valve performance: a fluid-structure interaction analysis. *Computer Methods in Biomechanics and Biomedical Engineering*, 24(4), 375-383.
- Nudel, I. (2015). *Characterization of the Mechanical Anisotropic Behavior of the Aortic Valve Leaflets*. Ben-Gurion University of the Negev, Faculty of Engineering Sciences, Department of Biomedical Engineering.
- Oks, D., Samaniego, C., Houzeaux, G., Butakoff, C., & Vázquez, M. (2022). Fluid–structure interaction analysis of eccentricity and leaflet rigidity on thrombosis biomarkers in bioprosthetic aortic valve replacements. *International Journal for Numerical Methods in Biomedical Engineering*, 38(12), e3649.
- Otto, C. M. (2008). Calcific aortic stenosis—time to look more closely at the valve. *New England Journal of Medicine*, 359(13), 1395-1398.
- Pandya, A. (2012). *Optimizing Cardiovascular Disease Screening and Projection Efforts in the United States* (Doctoral dissertation, Harvard University).
- Rubenstein, D., Yin, W., & Frame, M. D. (2015). *Biofluid mechanics: an introduction to fluid mechanics, macrocirculation, and microcirculation*. Academic Press.
- Sadrabadi, M. S., Hedayat, M., Borazjani, I., & Arzani, A. (2021). Fluid-structure coupled biotransport processes in aortic valve disease. *Journal of Biomechanics*, 117, 110239.
- Spühler, J. H., Jansson, J., Jansson, N., & Hoffman, J. (2018). 3D fluid-structure interaction simulation of aortic valves using a unified continuum ALE FEM model. *Frontiers in physiology*, 9, 363.
- Thubrikar, M. J., Aouad, J., & Nolan, S. P. (1986). Patterns of calcific deposits in operatively excised stenotic or purely regurgitant aortic valves and their relation to mechanical stress. *The American journal of cardiology*, 58(3), 304-308.
- Thubrikar MJ (1990) The aortic valve. CRC Press Inc., Boca Raton
- Wang, R., 2015. GrabCAD - CAD library. Grabcad.com. Available at: <<https://grabcad.com/library/aorta-aortic-valve-1>> [Accessed 01 January 2021].